 ICES-2018-320

Continued Development of a Liquid Amine Carbon Dioxide Removal System for Microgravity Applications

Giraldo Alvarez[1]
Jacobs Technology, Inc., Houston, Texas, 77058

Geoff DeGraff[2]
Barrios Technology, Inc., Houston, Texas, 77058

Michael J. Swickrath[3]
HX5, LLC, Houston, Texas, 77058

Grace Belancik[4]
NASA, Moffett Field, CA, 94035

and

Jeffrey J. Sweterlitsch[5]
NASA Johnson Space Center, Houston, TX, 77058

Carbon dioxide (CO_2) can rapidly accumulate in spacecraft, creating a dangerous breathing environment if not properly controlled. Traditionally, solid adsorbents have been used to capture and release the CO_2 generated by crew metabolic activity. Liquid absorbents have generally been avoided, due to the added complexity of handling fluids in a microgravity environment. However, with the advent of advanced manufacturing techniques using three-dimensional printing, a capillary-based gas/liquid contactor and degasser system has been developed and tested. Test data and an accompanying mathematical model have been developed for the contactor portion of the system. Flux rate data were then used to size a concept for application in a spacecraft. Finally, an integrated test stand was configured with the degasser and thermal control equipment. The integrated test stand was operated in a bench-scale format, confirming that the sizing analyses are realistic. A process model for the overall system developed in previous efforts was updated with all of the data collected during the most recent fiscal year. In aggregate, the results of parallel experimentation and modeling efforts continue to be encouraging for alternative liquid amine-based CO_2 capture system.

Nomenclature

ACM	=	Aspen Custom Modeler software package
CAD	=	Computer Aided Drafting
CO_2	=	Carbon Dioxide
CSTR	=	Continuous Stirred Tank Reactor
DGA	=	Diglycolamine
JSC	=	Johnson Space Center
LEO	=	Low-Earth Orbit
LiOH	=	Lithium Hydroxide

[1] Engineering Technologist, Crew and Thermal Systems Division, 2101 NASA Parkway/EC3
[2] Mechanical Engineer, Crew and Thermal Systems Division, 2101 NASA Parkway/EC3
[3] Chemical Process Simulation Engineer, Thermal and Environmental Analysis Section, 2224 Bay Area Blvd
[4] Physical Scientist, Bioengineering, Mailstop 239-15
[5] Research Engineer, Air Revitalization Technology Development, 2101 NASA Parkway/EC3

MDEA= Monodiethanolamine
MEA = Monoethanolamine
SMAC= Spacecraft Maximum Allowable Concentration

I. Introduction

NASA continues to aggressively develop capabilities for future space explorations to the moon and Mars. These destinations involve travel beyond low-Earth orbit (LEO) where resupply of oxygen (O_2) is logistically challenging. As a result of the new demands, NASA seeks to further close the material balance derived from metabolic respiration where oxygen is consumed generating carbon dioxide (CO_2) and water (H_2O). CO_2, in particular, can accumulate in a cabin causing crew to experience hypercapnia which presents itself through a number of symptoms: cognitive deficiencies, reduced visual acuity, shortness of breath, and headaches, to name a few[1].

The safe spacecraft maximum allowable concentration (SMAC) for CO_2 for space exploration is 5.2 mm Hg and the 1000-day limit is 3.6 mm Hg (see Table 4.2 of Anderson, 2015).[2] However, recent data suggests detrimental effects of CO_2 can manifest at levels as low as 0.8 mm Hg.[3] In lieu of such findings, NASA has increased its scrutiny of appropriate SMAC values and is considering targeting values of 2.0 mm Hg, and below, for the time-averaged mission.[4,5]

To mitigate CO_2 toxicity, we present experimental data and modeling results for a liquid amine chemisorbent CO_2 removal system. The system relies on two critical components: (1) a gas-liquid contactor which passes cabin air over a large number of grooved-trays filled with amine sorbent and (2) a degasser unit which again relies on a grooved structure for fluid transport, but the chemisorbent is heated for thermal regeneration.

The amine-based concept was previously reported as a chemical process model which suggested the technology shows merit for continued development.[6] In particular, the dynamics of CO_2 accumulation depended on cabin volume, crew metabolic activity, and gas flow through the contactor. Over the course of a parametric analysis though, there were configurations that could keep the daily average CO_2 level below the most aggressive 2.0 mm Hg target (see Rogers, *et al.*, 2018; Figure 11).[6] However, these results relied upon CO_2 capture dynamics that were predicted in a rigorous finite element method model developed in the COMSOL Multiphysics (COMSOL, Inc.; Burlington, MA) software package. That is, experimental data were needed to ensure flux rate calculations for the process model were reasonable which did rely on some approximations regarding what the gas/liquid interface within the grooves would look like. Efforts to collect these data were performed through the previous year.

Substantial progress has been made in prototyping and testing the most critical components within the design. In addition, the process flow diagram previously presented has been modified as shown in Figure 1. The most important changes to the process diagram are that the amine tank has been moved from downstream to upstream of the contactor. Also, a condensing heat exchanger has been added after the hot degasser to reclaim water vapor lost from the sorbent at high temperatures used during regeneration.

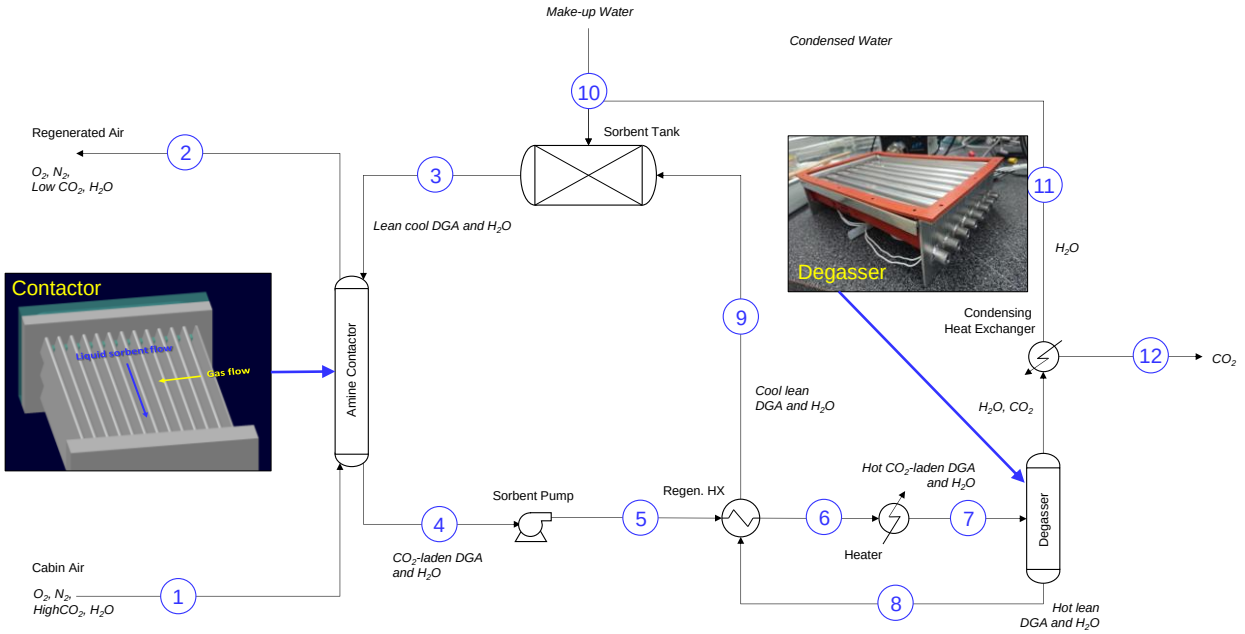

Figure 1. Liquid amine CO_2 capture process with insets demonstrating the gas/liquid contactor and one degasser prototype.

Since the previous modeling exercise,[6] much experimental progress has been made on the first-of-a-kind aspects of this system (namely, gas/liquid contactor and degasser). This document summarizes the findings for flux rate during CO_2 capture and desorption. In addition, a rigorous gas/liquid interface calculation has been performed and applied within a model to predict capture dynamics. Finally, preliminary degasser model data has also been collected and a summary will be discussed.

II. Governing Principles for Mass Transfer and CO_2 Equilibria

Carbon dioxide capture and release within the system (see Figure 1) is a multistep process involving a number of important steps for phase exchange, reaction, and careful thermal control. The process is cyclical and is illustrated in Figure 2. First, CO_2 starts out in vapor-phase in close proximity to the liquid film.

In the second step, some of the CO_2 in the vapor-phase will physically absorb into the liquid. Physisorption of CO_2 is rate limiting, in large part, because diffusion from the surface into the bulk liquid is quite slow given the orders-of-magnitude higher viscosity in the chemisorbent versus vapor viscosity. Thus, the weakly soluble physisorbed CO_2 collects at the gas/liquid interface (although rate limitations are ultimately mitigated by chemical conversion of CO_2 to other compounds as will be discussed shortly). The dynamics of this process are usually captured using a mass transfer coefficient k_m (in m/s), which is a parameter that is unknown *a priori*, but is typically calculated using correlations for the dimensionless Sherwood number, $\mathrm{Sh} = k_m L/D$. The Sherwood number is a ratio of convective to diffusive mass transport where D is the diffusion coefficient for CO_2 in air (0.16 cm^2/s) and L is the characteristic length-scale (tray spacing was used here). In some circumstances, the mass transfer coefficient can be further deconstructed where $k_m = k_{m,o}/a_s$ with $k_{m,o}$ as the inverse of a time constant (1/s) and a_s is the specific area under analysis where $a_s = A/V$ (area divided by volume in m^2/m^3). An excellent review of mass transfer processes can be found elsewhere,[7] which also provides a number of relationships to estimate k_m (see pages 5-59 to 5-68). Tables of Sherwood number formulae exist from literature studies over the course of decades;[7] however, these relationships only hold under specific conditions which may not be suitable for the first-of-a-kind technology developed by NASA. In the case of initial testing, 10 separate relationships were identified as potentially appropriate in our application. It was later found that Froessling relationship below most accurately calculated the dynamics of CO_2 mass transfer to the liquid-phase in the application described herein.

$$\mathrm{Sh} = 0.6 + \mathrm{Re}^{1/2}\mathrm{Sc}^{1/3} \quad (1)$$

In the Froessling equation, the Reynolds number is $\mathrm{Re} = \rho v L/\mu$, where ρ is the gas density (kg/m^3, calculated with the ideal gas equation of state), μ is the gas dynamic viscosity (Pa-s or kg/m-s), v is the gas interstitial velocity (m/s calculated by the volumetric flow rate divided by the cross-sectional area and void fraction of the contactor), and L again is the characteristic length scale (tray spacing, m). Finally, the Schmidt number is $\mathrm{Sc} = \mu/(\rho D)$.

Solubility of physically absorbed CO_2 in the liquid-phase was calculated using a Henry's law approach. As will be discussed later, absorption rate will be calculated by a product of mass transfer coefficient and the difference between equilibrium CO_2 concentration from Henry's law and actual concentration (the departure from equilibrium approach). Data for Henry's law solubility in DGA were collected from Chen, *et al.*[8]

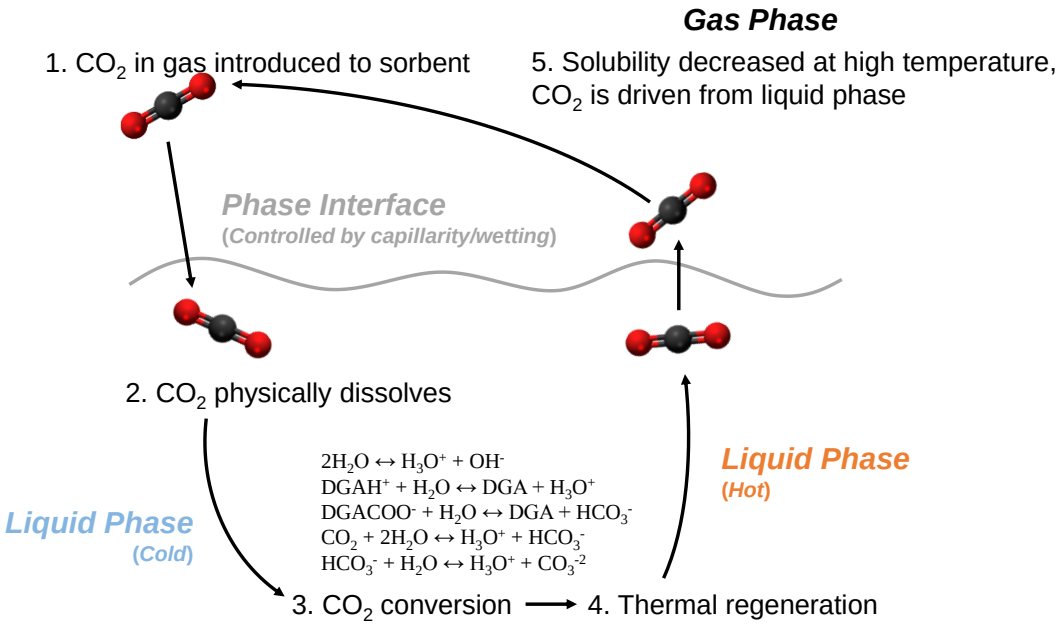

Figure 2. CO_2 capture and release cycle for the diglycolamine chemisorbent.

The third step involves the conversion of CO_2 to a number or other products or complexes. This step is key in the process because it ensures any physisorbed CO_2 converts to another product before reaching CO_2 saturation in the sorbent which would otherwise end the absorption process. A series of five parallel reactions, each of which has its own equilibrium coefficient,[9] take part within this step. The second and third reactions represent amine protonation[10,11] and amine-carbamate formation[12] while the remaining reactions are all associated with acid/base chemistry between CO_2 and H_2O.

The fourth step, regeneration, drives the equilibrium equations back to the formation of physically absorbed CO_2 via heating. Finally, the fifth step involves phase exchange of CO_2 between liquid/gas once again. Using the Henry's law approach developed by Chen, *et al.*,[8] it is found that only 28% of the CO_2 that is soluble at 25°C is soluble at 105°C (the current desorption temperature of interest). Initial test data and process simulation has indicated substantial water vaporization. This has been addressed by adding a condensing heat exchanger to the process diagram which did not exist in previous work.[6]

All of these steps require careful consideration for the optimization of CO_2 capture and release with an amine chemisorbent. Gas phase convection and diffusion need balanced to ensure bulk CO_2 can contact the interface. Gas/liquid contact area needs maximized during capture/desorb steps. Careful thermal management needs performed to ensure energy requirements and water vapor losses are minimized. And finally, the important components ultimately need to be coupled with balance-of-plant hardware in a packageable format (which has not been thoroughly addressed at this stage).

The focus of this work involves preliminary testing to support early-stage modeling efforts previously reported.[6] Some initial CO_2 flux results seemed to indicate early modeling may have been overly optimistic. Moreover, sensitivities to gas/liquid flows were found. A modeling effort was performed, with a rigorous capillary transport interface calculation, that provides significant insight into the principles controlling this behavior. Lastly, initial

regeneration experiments were performed indicating that CO_2 rejection rates are commensurate with absorption rates which suggests the critical components of the system have dynamics in balance with one another.

III. Contactor Testing

In total, four separate gas/liquid subscale contactor prototypes were designed and fabricated through three-dimensional (3D) printing (3D Print Texas; Houston, TX). The printing material used was VeroClear™ (Stratasys Ltd.; Eden Prairie, MN) which is a transparent photopolymer that simulates polymethyl methacrylate (commonly referred to as acrylic). These prototypes are summarized below in Table 1.

Table 1. Summary of prototyped contactor units.

Unit	Purpose	Length, in.	Width, in.	Height, in.	Tray Spacing, in.	Trays	Grooves
Unit 1	Manufacturing	2.75	3.38	2.00	0.45	3	72
Unit 2	Unit 1 Modification	2.75	3.38	2.00	0.45	3	72
Unit 3	Testing	2.75	6.87	7.75	0.45	16	384
Unit 4	Testing	2.75	6.87	7.75	0.30	26	624

The first prototype (Unit 1) was an experiment in manufacturability ensuring the 3D printing process can print the small features within the prescribed design tolerances. Some efforts were made to flow liquid through the contactor but it was found that the manifold design did not introduce fluid in the correct manner to ensure adhesion of the liquid to the v-groove design. The second prototype (Unit 2) had the same dimensions of Unit 1 but had a modified manifold design which solved the fluid adhesion problem. The design for Unit 2 was tested and enabled controlled flow of water with dyes for visualization as well as 65vol% DGA balanced with water. Unit 3 involved upscaling the Unit 2 design to something expected to be appropriate for human metabolic CO_2 output. Substantial test data were collected with this design (as will be discussed later). After receiving initial test data, it appeared convective transport of CO_2 passing through the contactor had faster dynamics than diffusion of CO_2 from the bulk stream to the chemisorbent interface. As a result, Unit 4 relied on reduced tray spacing to ensure more CO_2 would transport to the liquid interface. This modification also increased the number of trays from 16 to 26 with the added benefit of increased gas/liquid contact area by 62.5%. In addition to geometric modifications, Unit 3 and Unit 4 were both tested under a number of process changes including parametric testing of both gas and liquid flow rates.

A general test stand, shown in Figure 3, was created to accommodate the current, and future, test articles for performance testing. This test stand is similar to a wind tunnel in the respect that test article could be inserted through a top opening and fixed to the midpoint of the test stand where air would flow through into and across the test article. This test stand had plenum adapters added on both sides to reduce and convert the 12×12 square to 4-inch round. A flow straightener was added to the inlet side to produce a uniform laminar flow entering the main duct. A carbon filter pad was added to the outlet of the test stand to reduce possible contamination at the outlet and a bilge blower was added to the inlet to create the process air flow stream. Two calibrated LI-COR 840A CO_2/humidity sensors (LI-COR Environmental, Inc.; Lincoln, NE) were added, one on each of the test article, to measure CO_2 and humidity concentrations. A Kanomax S-6541-0E hot-wire air anemometer (Kanomax USA; Andover, NJ) was inserted into the inlet side of the PVC tubing to enable flow rate adjustment.

A K-bottle containing 100% CO_2 was attached to the facility pressure system before the bilge blower to dial specific concentration challenges and to ensure mixing before the process flow stream entered the tunnel. The facility pressure system provided a needle valve upstream of the blower to regulate accurate concentrations of CO_2 for the process air. The CO_2 levels at the inlet of the tunnel were measured after mixing to ensure the desired CO_2 levels.

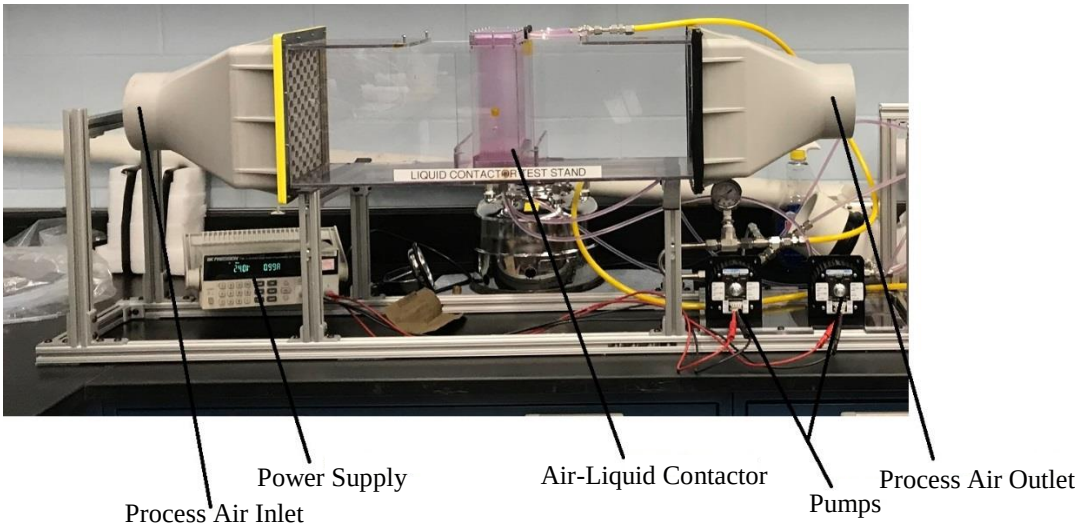

Figure 3. Liquid amine contactor test stand.

A cutout in the top of the square wind tunnel allowed the contactor to be placed through the top and into the path of the airstream. Since the tunnel was larger in cross-sectional area than the tested contactors, a chemical resistant plastic was used around the contactors that was smaller than the cross-sectional area to force the airstream into the path of the contactors.

Tubing, which was attached to a micropump, was inserted through the plastic tunnel to mate with the contactor inlet and outlets. A reservoir was attached to the outlet to simulate 500 mL working fluid which is half the currently proposed liquid volume for the final system.

The test stand did not have a CO_2 desorption system (regeneration capability) incorporated into its design at the time of initial testing, therefore the fluid was not regenerated during testing. Instead, a new batch of 65vol%:vol35%, DGA:H_2O, solution was created for each experiment. The solution was removed between each test and the duration of each test was approximately one hour long. Figure 4 demonstrates some sample data collected from the test stand.

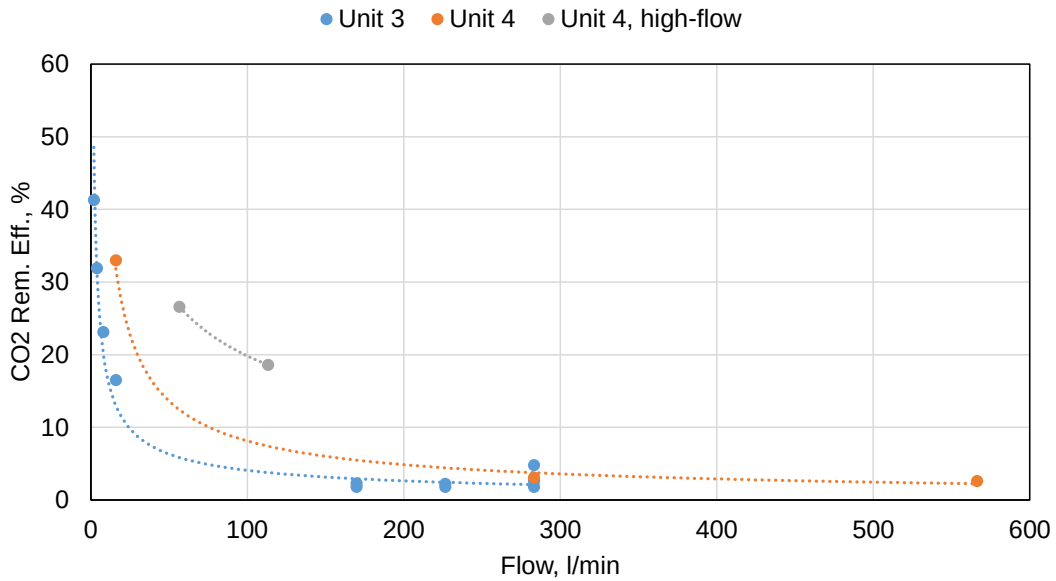

Figure 4. Removal efficiency for a variety of gas flow rates for contactors 3 and 4 with 100 ml/min sorbent flow for baseline cases and for contactor 4 at 1500 ml/min (high-flow).

As seen in Figure 4, removal efficiency (calculated as inlet CO_2 mass flow minus outlet flow divided by inlet flow) decays dramatically as the flow rate increases. The Unit 3 and Unit 4 data were collected at liquid sorbent flow rates of 0.1 L/min while Unit 4, high-flow was collected at 1.5 L/min. At gas flow rates expected as reasonable for space exploration (~26 acfm or 736.2 L/min), the removal efficiency was especially low (less than 5%); however, the flux rates were as high as 0.34 g/m^2-min, which will be used to scale up results for a full-scale reactor at a later time Scaling considerations will include known removal efficiency, overall gas flow rate, and surface area contacted for the gas surface based on design geometry and measured gas/liquid wetting interactions.

Moreover, for a contactor with a cross-sectional area of 53.2 in^2 (computed from Table 1), and a flow rate of 26 acfm (748.8 in^3/s), the superficial velocity would be 14.1 in/s leading to a residence time of 0.20 seconds through the 2.75 in long flow path. Given tray spacing is 0.30-0.45 inches (0.76-1.14 cm), and a diffusion coefficient of 0.16 cm^2/s, the characteristic diffusion time can be calculated as $\tau_d = L^2/(4D)$ which results in 0.91-2.04 seconds representing the time required for a CO_2 molecule between two trays to travel to the liquid interface through diffusion alone. Increasing flow rate increases the Reynolds number which will also increase the Sherwood number; however, increased flow also decreases the residence time compared to diffusion time which severely impacts performance as evidenced by Figure 4. The finding of this analysis is that decreasing flow to maximize removal efficiency is likely not a viable solution as throughput requirements could not be met. Instead, it is likely a low removal efficiency should be offset by scaling the size of the contactor so that sufficient area exists to support the necessary flux for a safe atmosphere. These simple scaling calculations demonstrate the gas flow through the contactor is sufficiently high that only CO_2 closest to a tray interface can be absorbed. Two design changes can be made to improve removal efficiency which both rely on increasing area to improve flux: (1) reduce spacing between trays, and (2) lengthen the flow path through the contactor. The first design change was performed in between contactor 3 and 4 and little room is left to pack additional trays. The second design change is under consideration as scale-up activities are underway.

IV. Degasser Testing

In addition to iterating the design of the contactor to capture CO_2, there must also exist a method to efficiently regenerate the chemisorbent and to reject the CO_2 to space, or to store elsewhere so that the CO_2 can be used to in other ways to further close the life support system material balance (*e.g.*, Sabatier or Bosch reaction). To evaluate regeneration and associated mass transfer rates, a single V-Tube test article was made as illustrated in Figure 5.

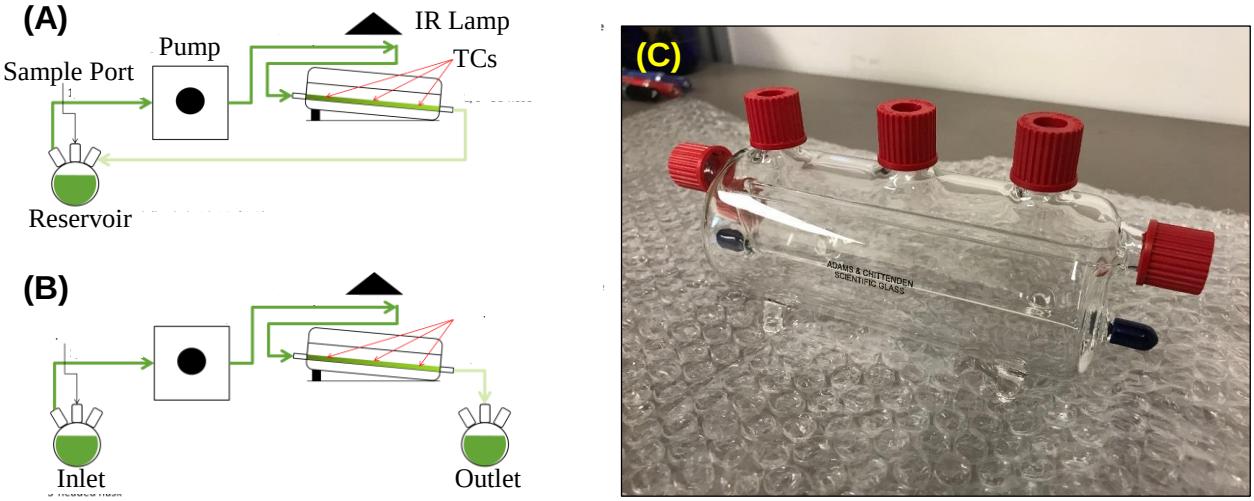

Figure 5. V-Tube experimental configuration for (A) closed-loop operation and (B) open-loop operation. (C) V-Tube test article.

The V-Tube is constructed of an enclosed glass flask with multiple ports for thermocouples and for evolved CO_2 to exit. Within the flask, a single glass V-groove is placed. The main design of the V-Tube system follows the same geometry of the contactor, using a sharp-angled inner corner channel to contain the liquid. However, the angle of the channel is sharper, 15°, to maintain wetting characteristics as surface tension decreases at elevated temperatures. An infrared lamp positioned roughly 5.5 inches from the liquid surface was responsible for thermal regeneration within this design.

The V-Tube was operated in two separate configurations. These included closed-loop (Figure 5A) and open-loop (Figure 5B) configurations. In closed-loop operation, the sorbent is continuously cycled from the V-Tube outlet back into the sorbent reservoir. Aliquots of sorbent were taken from the reservoir periodically for measuring CO_2 concentration via FTIR. During open-loop configuration, after all the sorbent flows through the V-Tube and is collected in a separate container, it is plumbed back into the inlet. Aliquots of sorbent were taken from the outlet container for measuring CO_2 concentration via pH desorption.

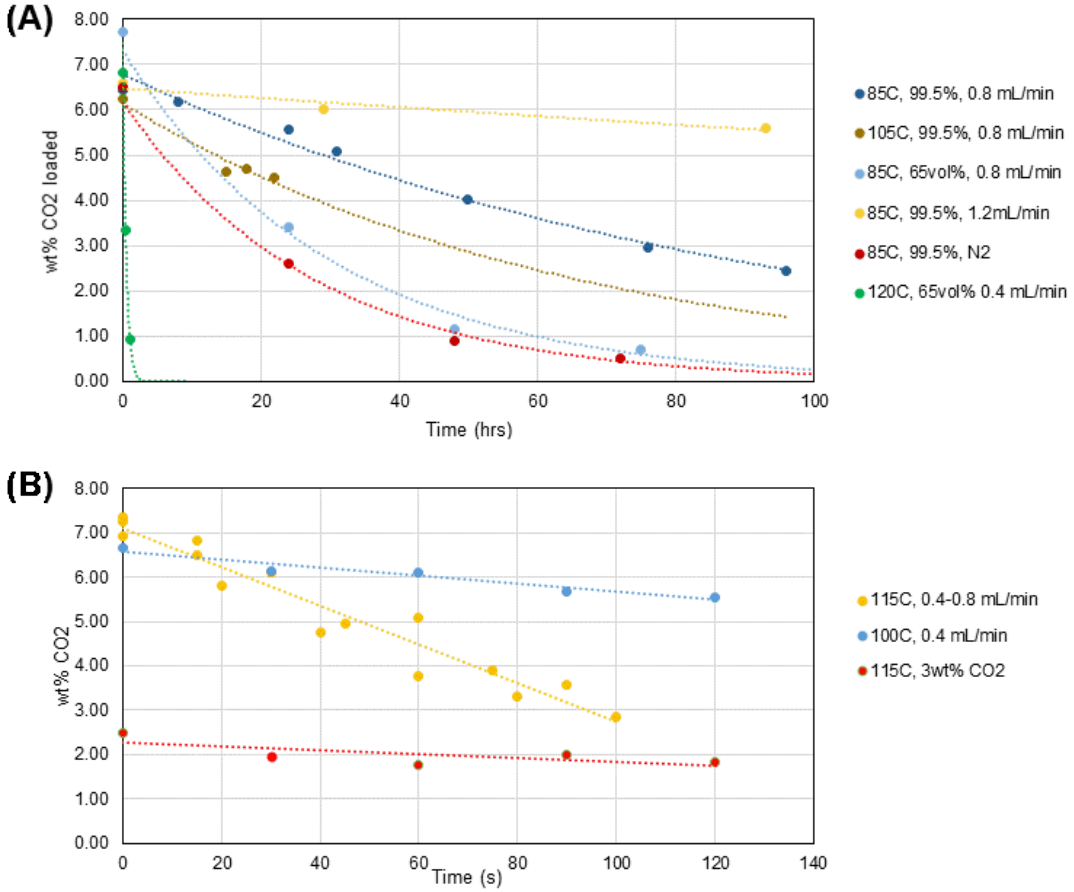

Figure 6. Results for V-Tube degassing experiments under various conditions in both (A) and closed-loop and (B) open-loop configurations.

Initial desorption results with the closed system at 0.8-1.2 ml/min sorbent flow (99.5wt% DGA), starting from a CO_2-saturated condition (~7wt%), at 85°C showed very slow desorption results (Figure 6A). These data gave rise to a few hypotheses. First, it was speculated that evolved CO_2 was remaining within the headspace, which leads to a higher equilibrium amount of CO_2 in the liquid phase as would be predicted via Henry's law. To inhibit this effect, a nitrogen (N_2) sweep gas was introduced in the headspace. This resulted in a dramatic increase in regeneration rate, however, utilizing a sweep gas in future systems would not be practical as it dilutes the CO_2 product. Another concern was that the viscous DGA was slowing diffusion of bulk CO_2 transfer to the interface. To improve desorption kinetics, the solution was diluted to 65wt% DGA balanced with water, which also appreciably changed the desorption rate. Finally, the temperature of desorption was increased as high as 120°C, resulting in an order of magnitude faster desorption kinetics. Although the kinetics were fast, rapid water boiling was observed. Further discussion on this system testing and determination of CO_2 concentration can be found in Huang, et. al. 2018.[13]

In order to run the V-tube in a more system-like configuration, i.e. simulating the fluid coming from the contactor rather than mixing into a reservoir with higher CO_2-loaded DGA, the system was also operated in an open-loop configuration. These results are displayed in Figure 6B. In this format, regeneration was reduced from many hours to many seconds. Flux rates for these experiments are summarized elsewhere,[14] but were found, in some cases, to far exceed flux rates collected on the contactor which suggests that the degasser will be able to maintain kinetics commensurate with CO_2 capture rates. However, these tests will need to be repeated both in a larger scale desorption test system and in an integrated absorption/desorption test to be done at a later time to build confidence in the results.

V. CO_2 Capture Dynamics Model

Initial contactor test results have been collected under various conditions. Thus far, results have proven sensitive to both the air and chemisorbent flow rates. It is also apparent that contactor design influences performance as well. Given contactor prototyping and testing is a time-consuming endeavor, it would be advantageous to have a mathematical model that can provide insight on performance characteristics as designs and process parameters are changed. The following sections describe the current state of a model developed in parallel to testing efforts.

A. CO_2 Mass Transfer and Reactive Conversion

The rate of CO_2 uptake in the chemisorbent is of critical interest considering its importance with regard to sizing a contactor for a crew of four. In this analysis, a mass transfer model was employed which has heritage in analogies to heat transfer[15,16]. The model was originally designed to treat cross-flow hollow fiber membranes, similarly to heat exchange in a cross-flow tube heat exchanger, but the method in which the geometry is generalized allows it to be used for the groove system within the contactor.

The model was derived using a few principal assumptions. First, transients are neglected and steady-state isothermal operation is assumed. The absorption reaction is exothermic. But given the low vapor phase concentration of CO_2, the heat generation is expected to be minimal. Secondly, the original mass transfer model by Dindore, *et al.*[15-16] neglected chemical reaction where we have instead adapted the model to include the chemical reaction most relevant to transport kinetics. Third, changes in volumetric flow are minimal (which is again expected due to trace concentrations of CO_2 being removed). Lastly, the overall mass transfer coefficient was treated as constant throughout the model. Since the mass transfer coefficient depends on physical properties and the flow rate, this assumption is likely valid as well since neither change appreciably with CO_2 removal.

With these assumptions, the model calculates the cross-sectional average composition gas and sorbent as the gas passes through the contactor. Figure 7 demonstrates the geometry associated with the model as viewed from the side (perpendicular to both gas and sorbent flow). As shown in Figure 7, the process air flows in through the left-side leaving out the right-side. Liquid amine is then sent from the top manifold downward along the v-grooves to the bottom manifold. The direction of flows in Figure 7 are strictly for illustration purposes and have no bearing on how the contactor needs to be oriented for microgravity application.

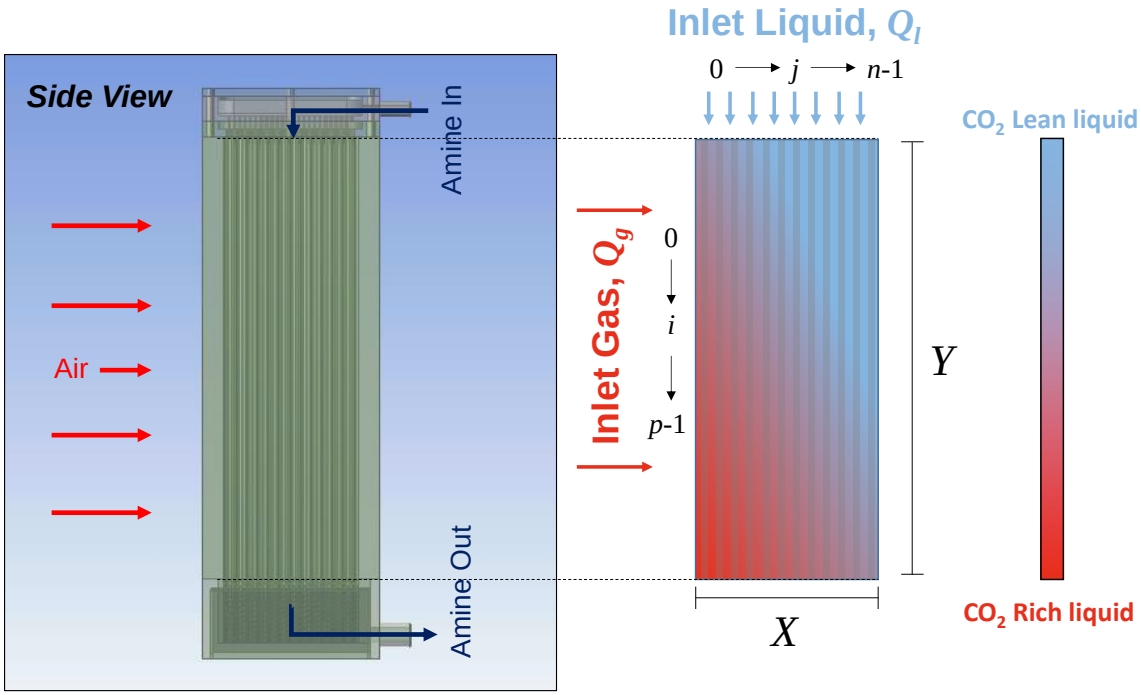

Figure 7. Representation of gas/liquid contactor and its relation to the mass transfer model employed for performance predictions.

The equations derived for CO_2 capture in hollow fiber membranes are displayed below.[16]

$$\frac{\partial C_g}{\partial y} = -\frac{k_m X}{Q_g}(C_l^* - C_l) \tag{2}$$

$$\frac{\partial C_l}{\partial x} = \frac{k_m Y}{Q_l}(C_l^* - C_l) \tag{3}$$

In the above, C_g is the gas-phase CO_2 concentration (moles/liter), C_l is the liquid-phase CO_2 concentration (moles/liter), C_l^* is the liquid-phase CO_2 concentration at equilibrium conditions (moles/liter), X and Y are the contactor dimensions (meters) in the corresponding x and y directions, and Q_g and Q_l are the gas and liquid volumetric flow rates (m^3/s), respectively. Finally, k_m is the mass transfer coefficient calculated from a Sherwood number correlation (see equation 1). The equilibrium concentration in the liquid-phase is calculated from Henry's law using data from Chen, *et al.*,[8] based on gas-phase partial pressure P_c, and the Henry's law coefficient k_H, $C_l^* = P_c/k_H$.

It should be noted that the actual X dimension, in the direction perpendicular to the liquid flow, depends on the y distance down the contactor. That is, the liquid filament within each groove takes on a location-specific shape which depends on liquid flow rate, fluid properties, and fluid substrate interactions. This effect is important in capturing performance predictions and will be explained in detail in a later section of this report.

If physical absorption were the only driving force for CO_2 transport, and since CO_2 is only slightly soluble in DGA/H_2O, the total capacity of the chemisorbent would be small. Instead though, CO_2 dissolves and then reactively converts to an amine carbamate salt. There are five reactions responsible for this process; however, to simplify matters, the five reactions were summed and modeled as a single overall reaction:

$$\mathrm{DGA} + \mathrm{CO_2} + \mathrm{H_2O} \leftrightarrow \mathrm{H_3O^+} + \mathrm{DGACOO^-} \tag{4}$$

A rate law was introduced for this reaction where the reaction rate r (mol/liter-second) was modeled based on component concentrations C_i in the liquid-phase using CO_2 concentration (denoted with l) and DGA (denoted with d).

$$r = kC_lC_d \tag{5}$$

$$k = k_\circ \exp\left(-\frac{E}{RT}\right) \tag{6}$$

In the above expression, k is the reaction rate constant which is calculated using the Arrhenius expression with E representing the reaction activation energy. The parameters for this expression were published elsewhere[17] as $k_o = 5.98 \times 10^{18}$ liter/mol·s, $E = 15{,}813$ cal/mole, $R = 1.987$cal/mol·K.

Finally, the mass transfer model was updated to account for reaction resulting in the following relationships.

$$\frac{\partial C_g}{\partial y} = -\frac{k_m X}{Q_g}\left(\frac{P_c}{k_H} - C_l\right) \tag{7}$$

$$\frac{\partial C_l}{\partial x} = \frac{k_m Y}{Q_l}\left(\frac{P_c}{k_H} - C_l\right) - \frac{kC_lC_d}{v_l} \tag{8}$$

As discussed above, k_m is not known a priori and is instead calculated with a dimensionless Sherwood number calculation. During initial testing, the Froessling equation (equation 1) agreed best with experimental data for contactor unit 3. Since the model is two-dimensional in x, y directions, it does not capture the affect of increasing interfacial for contactor unit 4 which has 26 trays rather than 16. For unit 4, the mass transfer coefficient was increased by multiplying by a factor of the ratio of specific areas between contactor 3 and contactor 4 (where specific area is interfacial area divided by contactor volume which is essentially the ratio of 26/16 since unit 3 and 4 had equivalent volumes). Finally, a number of process parameters and physical properties were needed in this analysis. Relevant ranges and values are summarized in Table 2.

Table 2. Relevant values and ranges of physical properties and process parameters used in the model.

Variable	Explanation	Values/range
D_{CO2}	Diffusion coefficient for CO_2 in air at 20°C	0.16 cm^2/s
d_t	Tray spacing within a contactor design	7.6-11.4 mm
θ	Contact angle between sorbent and substrate	60°
α	V-groove half-angle	12.5°
k_m	Mass transfer coefficient, calculated	3.6-21.8 mm/s
Sh	Sherwood number, ratio of convective-to-diffusive transport	2.6-10.3
Sc	Schmidt number, ratio of momentum-to-mass diffusivity	0.95
Re	Reynolds number, ratio of inertial-to-viscous forces	1-198
v_g	Gas superficial velocity	1-397 mm/s
ρ_g	Gas density, from ideal gas equation of state	1.2 kg/m^3
μ_g	Gas viscosity	1.81×10^{-5} Pa-s

B. Gas/Liquid Capillary Interface Model

To accurately calculate the flux of CO_2 into the DGA/water sorbent, the actual gas/liquid interfacial area needs to be calculated. The capillary shape within a V-groove was rigorously analyzed in an effort to update the liquid filament width and gas/liquid interfacial distance (captured by X). The geometry under analysis is represented by Figure 8. It should be noted that this analysis holds under conditions in which surface tension is capable of overcoming gravitational forces. Such an assumption is validated using the Bond number which is a dimensionless group relating surface tension to gravitational forces, $\mathrm{Bo} = \Delta\rho g L^2/\sigma$. In the case of this technology, under terrestrial conditions, the Bond number is approximately $\mathrm{Bo} = (1000\ \mathrm{kg/m^3})(10\ \mathrm{m/s^2})(0.001\ \mathrm{m})^2/(0.072\ \mathrm{kg/s^2}) = 0.14$. Under microgravity conditions, the Bond number is lower. In other words, the geometry used within the contactor should be insensitive to gravitational conditions in terrestrial testing and microgravity application.

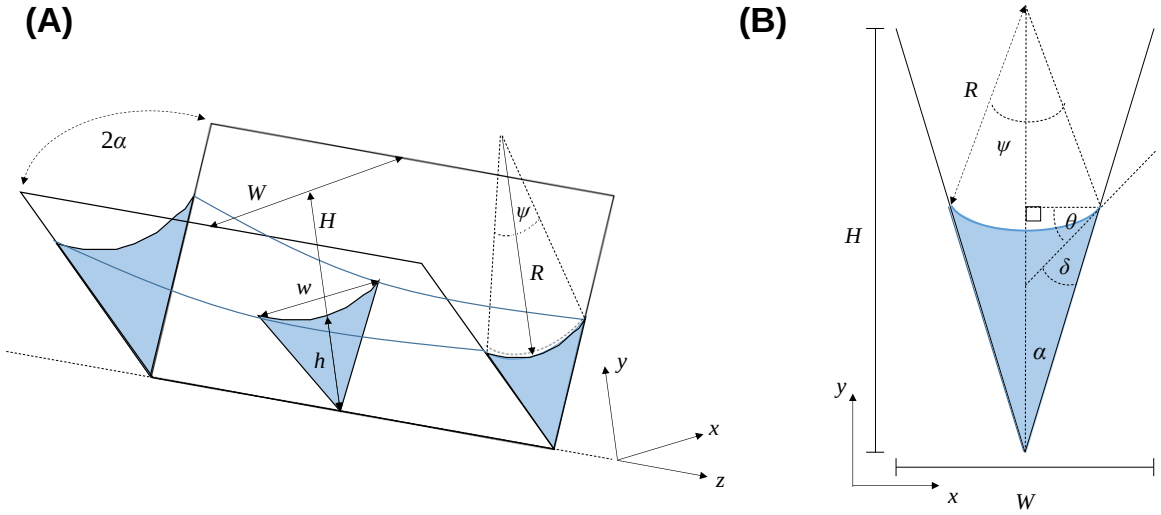

Figure 8. Illustration of capillary filament traversing v-groove.

In this figure, there is a V-groove of width W, height H, which has a half-angle α, where $\tan\alpha = H/(W/2)$. Liquid/substrate interactions, usually represented by surface tension and surface energy, give rise to a characteristic contact angle θ. The filament surface curves and can be fit by a radius of curvature R that is an outcome of the contact angle θ. There is a final angle ϕ that can be calculated knowing that the sum of all angles within a triangle is equal to 180° or π.

To calculate the radius of curvature, first it is fit to the equation for a circle (which is generally a good approximation but not entirely rigorous; see Chapter 2, sections 1 and 2 of Adamson & Gast[18]).

$$x^2 + (y - h - r)^2 = r^2 \tag{9}$$

This equation is solved for y as a function of x. The derivative of the resulting function is the slope of the V-groove wall which is equal to $\tan(\pi/2 - \theta)$.

$$y = h + r - (r^2 - x^2)^{1/2} \tag{10}$$

$$\frac{dy}{dx} = \frac{x}{(R^2 - x^2)^{1/2}} = \tan(\pi/2 - \theta) \tag{11}$$

The wall can also be parameterized by the line $y = (2H/W)x$. This relationship is inserted in the above to eliminate x and then the equation is solved for R as a function strictly of geometry and wetting characteristics between fluid/substrate.

$$R = \left(\frac{W^2}{4} + \frac{W^2}{4\tan^2(\pi/2 - \theta)}\right)^{\frac{1}{2}} \tag{12}$$

Once the radius of curvature is known, the liquid height as a function of distance must be calculated. On the inlet side, the fluid is actively pumped into the groove creating a higher pressure as a driving force mobilizing the fluid. As the fluid flows across the groove, capillarity within the groove assists with fluid flow while viscous resistance and friction with the wall oppose the flow. The analysis within this section draws largely from the comprehensive work of Weislogel.[19] For capillarity to occur within the geometry illustrated in Figure 8, the Concus-Finn condition must be satisfied: $\theta < \pi/2 - \alpha$.[20-22] If this condition is met, the fluid will wet the V-groove in accordance with Figure 8. If not, then the fluid can still be actively pumped into the grooves but will not adhere and wet the surfaces to generate a thin layer for optimal gas/liquid mass transfer.

A closed-form steady-state solution has been developed for fluid flow within a groove (see equations 2.89 and 2.90 of Weislogel).[19] For a groove of length L, the height at any z-location (from 0 to L) and the volumetric flow rate are determined.

$$h(z) = h_o\left[1 - \frac{z}{L} + \frac{z}{L}\left(\frac{h_L}{h_o}\right)^3\right]^{1/3} \tag{13}$$

$$Q = \frac{GF_A h_o^3}{3L}\left[1 - \left(\frac{h_L}{h_o}\right)^3\right] \tag{14}$$

In the above expressions, h_o and h_L are the centerline filament heights at $z = 0$ and $z = L$, respectively. In our case, Q is experimentally set (ranging from 0.1-2.0 liters/minute). Also, h_o is unknown but approximated. Then h_L is calculated and h_o is iteratively changed until h_L is just above zero at L which is the condition when the fluid can begin exiting the V-groove.

A few other parameters must be calculated to enable this analysis. Specifically, F_A is a geometry-dependent cross-flow area function and G is a dimensionless flow coefficient, and f is a surface curvature function.

$$F_A = \frac{f^2 \sin^2\delta}{\tan\alpha}\left[1 - \left(\frac{2\delta - \sin 2\delta}{1 - \cos 2\delta}\right)\tan\alpha\right] \tag{15}$$

$$G = \frac{\sigma F_i \sin^2\alpha}{\mu f} \tag{16}$$

$$f = \frac{\sin\alpha}{\cos\theta - \sin\alpha} \tag{17}$$

In the expression for G, σ is the liquid surface tension (N/m), μ is the dynamic viscosity (Pa-s), and F_i is referred to as the banded flow resistance function.

$$F_i = \frac{f^2}{\beta \sin^2\alpha} \tag{18}$$

The parameter β is the dimensionless flow resistance which is determined from tables (see Table 2.2 of Weislogel),[19] numerically, or through correlations. Herein, a correlation was used for β published elsewhere.[23,24]

$$\beta = \exp\left(\frac{b + 2d\alpha}{1 + 2c\alpha}\right) \tag{19}$$

In the above equation, a factor of 2 arises simply due to a difference in specifying a half- versus full-angle. The values of other parameters are $b = 2.124$, $c = -0.00415$, and $d = 0.00783$. This empirical function was found to produce a goodness of fit coefficient of 0.995 against a numerical table of data.[23]

At any given z-location, the value of h is now determinable which represents the centerline height. To calculate the area of the filament though, it is also necessary to know the points at which the filament and wall make contact. Those points are denoted as the tuples $(-w^+/2, h)$ and $(w^+/2, h)$ as shown in Figure 9 which are a small distance from $(\pm w/2, h)$. This distance may or may not be negligible depending on the contact angle for the fluid/substrate pair. Specifically, in the limit that $\theta \to \pi/2$, $(\pm w^+/2, h^+) \to (\pm w/2, h)$.

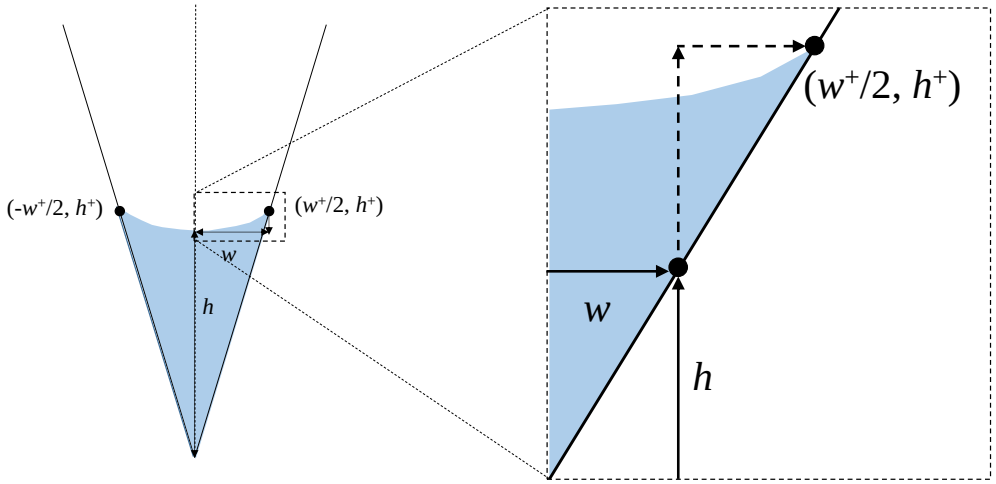

Figure 9. Location of contact points between filament and wall.

The determination of the intersection is solved for by using the linear parameterization of the wall and the circular fit to the curve filament gas/liquid interface.

$$\frac{2H}{W}x = h + R - (R^2 - x^2)^{1/2} \tag{20}$$

This relation is expanded to a second-order polynomial formula in terms of x where the solution for x is w^+.

$$\left(\frac{4H^2}{W^2} + 1\right)x^2 + \left(-\frac{4hH}{W} - \frac{4RH}{W}\right)x + (h^2 + 2hR) = 0 \tag{21}$$

This relationship is solved with the quadratic equation. It has been found that the physical root takes the only one of the two potential solutions.

$$w^+ = \frac{-\left(\frac{4H^2}{W^2}+1\right) - \sqrt{\left(\frac{4H^2}{W^2}+1\right)^2 - 4\left(\frac{4H^2}{W^2}+1\right)(h^2+2hR)}}{\left(\frac{8H^2}{W^2}+2\right)} \tag{22}$$

There is also an angle ψ that can be made from $-w^+/2$ to R to $w^+/2$ (see Figure 9) that is used to calculate the length of the circular segment, $2sin\psi = w^+/R$. With the value of ψ, the length of the segment is $L_c = R\psi$. Finally, the surface area of the filament A_f, is calculated by integration across the filament length.

$$A_f = \int_0^L L_c dz \approx \sum_n L_{c,n}\Delta z \tag{23}$$

The solution implemented in this report involved numerical integration by dividing the domain into n equally-sized segments of length Δz and summing the product of $L_{c,n}\ \Delta z$.

The solution to these equations for two separate cases are demonstrated in Figure 10 for two flow rates employed during testing (0.1 liters/minute and 1.5 liters/minute). For the low flow rate, the viscous resistance and the hydrodynamic forces through an increased upstream pressure are relatively matched and the fluid at the inlet only accumulates to about 34% up the inlet. Over the course of the groove, the height of the fluid reduces slightly. In comparing the gas/liquid interfacial area versus a completely filled channel, the 0.1 liter/minute case has 26.2% of the area of the filled channel. Conversely, in the higher flow case, fluid is pumped into the channel at a rate in which viscous resistance is not as well matched and the fluid begins to accumulate in the front of the groove. The result is that the greater fill depth across the channel leads to an interfacial area of 69.3% of a filled channel. The model predicts that for flow rates in excess of 2.1 liters/minute, the inlet height exceeds groove height and the fluid would spill over. The spillage finding has not been verified experimentally although the overall relationships were compared against data previously presented for V-grooves and agreement was very good.[25] In addition, viscosity and surface tension are weakly sensitive to CO_2 absorption which has not been accounted for herein which do influence the dimensionless flow resistance parameter.

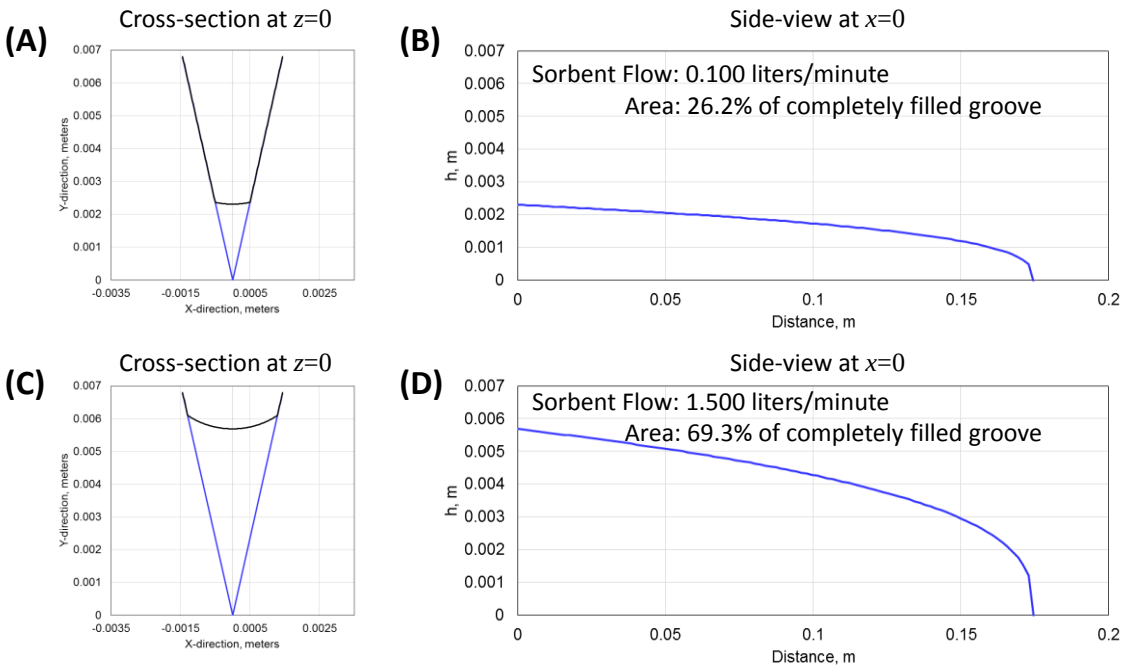

Figure 10. Sample results showing interfacial shape changes for two flow rates. (A, B) front view and side view for 0.1 liter/minute flow. (C, D) front view and side view for 1.5 liter/minute flow.

This model indicates flow rate does have a strong impact on the gas/liquid interface corroborating experimental findings. The next section of this document will compare performance results as a function of gas and liquid flow and with two separate contactor designs.

C. Comparison to Experimental CO_2 Capture Results

A detailed mass transfer and capillary wetting model has been established herein. The capillary wetting model, and the coupled set of ordinary differential equations for the mass transfer model, were solved numerically using the Python 3.0 computing language using the Anaconda Python distribution for scientific computing (Anaconda, Inc.; Austin, TX). The PyCharm v2017.1 integrated development environment (JetBrains S.R.O; Prague, Czech Republic) was used to develop code, to manage repositories, and to facilitate debugging and execution operations. For each contactor case, the Sherwood number was parameterized into 100 equidistant cases from a gas flow rate of 0.1 acfm to 26 acfm (Sherwood numbers 2.2-12.5). The parametric analyses were performed in batches of 300 (for Unit 3, Unit 4, and Unit 4 high-flow) which required roughly 45 minutes of compute time. These data are presented in Figure 11.

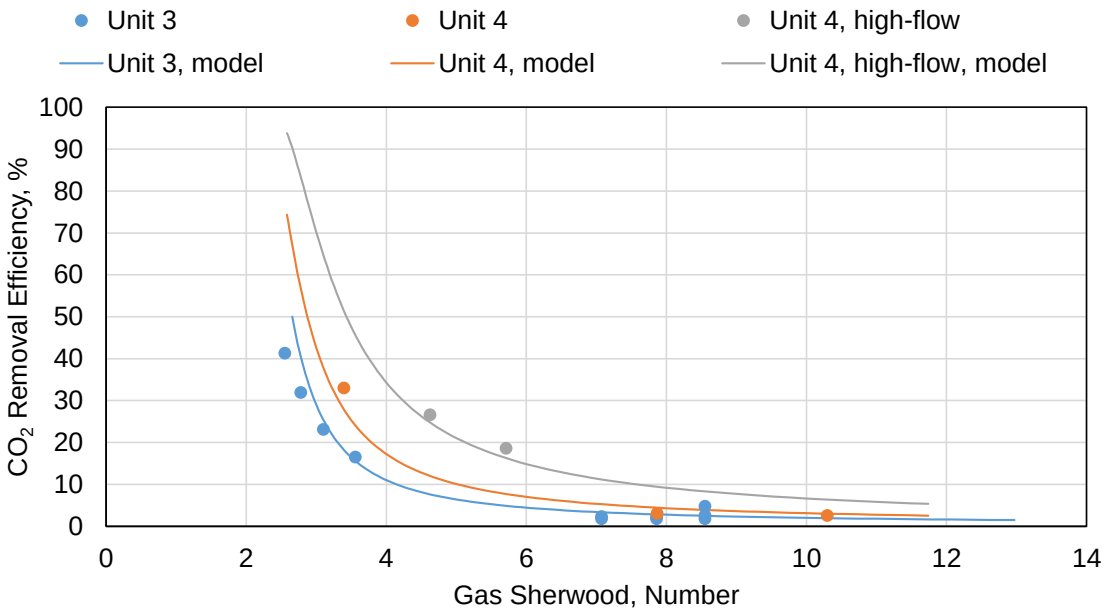

Figure 11. CO_2 removal efficiency as a function of contactor design, and gas/liquid flow rates. Unit 3 and Unit 4 data were collected with sorbent flow rates of 0.1 lpm while Unit 4, high-flow was collected at 1.5 lpm.

As seen in Figure 11, agreement between the experiment and model are rather good. As indicated by the results, Unit 4 slightly outperforms Unit 3. This result is attributed to the narrower tray spacing (0.30 inches for Unit 4 versus 0.45 inches for Unit 3). The narrower spacing gives a shorter diffusion distance and also allows for including more trays within a contactor of an equivalent volumetric envelope.

Moreover, the comparison to the 1.5 L/min data (Unit 4, high-flow), a dramatic increase in removal efficiency is observed. This result is attributed to a larger volumetric fill of each triangular groove which can substantial increase the gas/liquid interfacial area (see Figure 10). All in all, the outcome of the model development exercise resulted in a predictive model that seems to capture the effects of tray design/spacing and gas/liquid flow rate with good agreement. The model therefore provides another tool in the development efforts of the liquid amine contactor system.

Lastly, though not reported herein, a degasser model is currently under development as well. The model has been summarized elsewhere.[14] However, since experimental data collection to validate the model is still underway, we are reluctant to provide too many details on the model and results.

VI. Conclusions & Future Work

This report extends on previously reported model predictions for a liquid amine contactor/degasser system for CO_2 removal.[6] After a year of additional development, substantial experimental data were collected to provide insight into performance. Although the experimental data did not corroborate early model predictions in terms of flux rates, a number of encouraging aspects were found.

First, both contactor and degasser experimental setups were independently developed and tested. The contactor was capable of removing measurable amounts of CO_2 and provided some initial insight into design changes to improve performance.

Second, a degasser was tested under a variety of liquid flow rates, with and without sweep gas, and using both open/closed-loop configurations. In closed-loop testing, regeneration speed ultimately requires hours of operation to measurably reduce CO_2 content in the sorbent. However, if the regenerated sorbent is not allowed to mix with the CO_2-rich reservoir, as in open-loop testing, time required to regenerate a sample of sorbent drops from hours to seconds. Additional improvements to regeneration time are achieved if a sweep gas is used, water is added, or a temperature of 115°C is maintained. Flux rates achieved were as high as 40 g/m^2-min (two-orders of magnitude higher than CO_2 capture in the contactor). Therefore, the degassing process is not expected to be the performance limiting portion of the system.

Finally, a detailed contactor mass transfer model was developed and compared against experimental data. The capillary flow model shows a distinct sensitivity of performance on the liquid flow rate. The overall mass transfer model agreed well with experimental data.

All of these findings in aggregate are providing new insight into the liquid amine CO_2 capture process. Further work is underway to test contactor/degasser in an integrated process. In addition, the modeling efforts are also being adapted as new data is collected.

References

[1]Lambertsen, C. J., "Carbon Dioxide Tolerance and Toxicity." *Institute for Environmental* Medicine, University of Pennsylvania, 1971.

[2]Anderson, M.S., "Life Support Baseline Values and Assumptions Document." National Aeronautics and Space Administration, Doc. No. NASA/TP-2015–218570, March 2015.

[3]Satish, U., Mendell, M.J., Shekhar, K., Hotchi, T., Sullivan, D., Streufert, S., Fisk, W.J., "Is CO_2 an indoor pollutant? Direct effects of low-to-moderate CO_2 concentrations on human decision-making performance." *Environmental Health Perspectives*, Vol. 120.12, 2012.

[4]Anderson, M.S., Sargusingh, M., Perry, J., "Evolution of Requirements and Assumptions for Future Exploration Missions." *47th International Conference on Environmental Systems*, ICES-2017-271, Charleston, South Carolina, July 16-20, 2017.

[5]Law, J., Baalen, M.V., Foy, M., Mason, S.S., Mendez, C., Wear, M.L., Meyers, V.E., and Alexander, D., Relationship Between Carbon Dioxide Levels and Reported Headaches on the International Space Station, JEOM, 56 (5), 2014, pp. 481-482.

[6]Rogers, T., Swickrath, M.J., Verduzco, R., Sharma, S., Graf, J., "Feasibility Assessment of Liquid Amine Carbon Dioxide Removal System for Microgravity and Terrestrial Applications." *48th International Conference on Environmental Systems*, ICES-2018-039, Albuquerque, New Mexico, July 8-12, 2018.

[7]Perry, R.H., Green, D.W., *Perry's Chemical Engineers' Handbook*, 8th Ed., New York: McGraw-Hill, 2008.

[8]Chen, C.C., Britt, H.I., Boston, J.F., and Evans, L.B., "Extension and Application of the Pitzer Equation for Vapor-Liquid Equilibrium of Aqueous Electrolyte Systems with Molecular Solutes." *American Institute of Chemical Engineers Journal*, Vol. 25(5), 1979, pp. 820-831.

[9]Wang, Z., Gupta, M., Warudkar, S.S., Cox, K.R., Hirasaki, G.J., Wong, M.S., "Improved CO_2 Absorption in a Gas-Liquid Countercurrent Column." *Industrial & Engineering Chemistry Research*, Vol. 55, 2016, pp. 1387-1400.

[10]Danckwerts, P. V. "The Reaction of CO2 with Ethanolamines." *Chemical Engineering Science*, Vol. 34, 1976, pp. 443–446.

[11]Caplow, M. "Kinetics of Carbamate Formation and Breakdown." *Journal of the American Chemical Society*, Vol. 90, 1968, pp. 6795–6803.

[12]Sartori, G.; Savage, D. W. "Sterically Hindered Amines for CO_2 Removal from Gases." *Industrial Engineering & Chemistry Fundamentals*, Vol. 22, 1983, pp. 239–249.

[13]Huang, R., Silveria, M., Kong, J., Belancik, G., Jan, D., "Efficacy of FTIR Analysis in Determining CO2 Loading on Diglycolamine." *48th International Conference on Environmental Systems*, ICES-2018-039, Albuquerque, New Mexico, July 8-12, 2018.

[14]Alvarez, G., Belancik, G., Swickrath, M.J., "2018 End of Year Advanced Exploration Systems Liquid Amine Report." National Aeronautics and Space Administration, Doc. No. CTSD-ADV-1574, October 16, 2018.

[15]Dindore, V.Y., and Versteeg, G.F., "Gas–liquid mass transfer in a cross-flow hollow fiber module: Analytical model and experimental validation." *International Journal of Heat and Mass Transfer*, Vol. 48, 2005, pp. 209-222.

[16]Dindore, V.Y., Brilman, D.W.F., and Versteeg, G.F., "Modelling of Cross-flow Membrane Contactors: Physical Mass Transfer Processes." *Journal of Membrane Science*, Vol. 251, 2005, pp. 3352-3362.

[17]Aspen Technology, Inc. "Rate-Based Model of the CO_2 Capture Process by Diglycolamine Using Aspen Plus," Version 8.6, 2014.

[18]Adamson, A.W., and Gast, A.A., "Chapter 2: Capillarity," Physical Chemistry of Surfaces, 6th Ed., John Wiley & Sons, Inc., New York: NY, 1997.

[19]Weislogel, M.M., "Capillary Flow in an Interior Corner," NASA Technical Memorandum, TM-107364, November, 1996.

[20]Concus, P., and Finn, R., "On Capillary Free Surfaces in the Absence of Gravity," *Acta Mathematica*, Vol. 132, 1974, pp. 177-198.

[21]Concus, P., and Finn, R., "On Capillary Free Surfaces in a Gravitational Field," *Acta Mathematica*, Vol. 132, 1974, pp. 207-223.

[22]Concus, P., and Finn, R., "On the Behavior of a Capillary Surface in a Wedge," *Applied Mathematical Sciences*, Vol. 63(2), 1969, pp. 292-299.

[23]Or, D., and Tuller, M., "Flow in Unsaturated Fractured Porous Media: Hydraulic Conductivity of Rough Surfaces," *Water Resources Research*, Vol. 36(5), 2000, pp. 1165-1177.

[24]Or, D., and Tuller, M., "Hydraulic Conductivity of Variably Saturated Porous Media: Film and Corner Flow in Angular Pore Space," Water Resources Research, Vol. 37(5), 2001, pp. 1257-1276.

[25]Viestenz, K.J., Jenson, R.M., Wielogel, M.M., "Capillary Structures for Exploration Life Support Payload Experiment," *48th International Conference on Environmental Systems*, ICES-2018-241, Albuquerque, New Mexico, July 8-12, 2018.